

Original Article



DNMT1 methylation of LncRNA-ANRIL causes myocardial fibrosis pyroptosis by interfering with the NLRP3/Caspase-1 pathway

Zuntao Liu^{1,2,#}, Lei Gao^{3,#}, Chenjing Kan⁴, Xin Chen⁵, Kaihu Shi^{1,2,*}, Wei Wang^{1,2,*}

¹ Department of Cardiothoracic Surgery, Affiliated Hospital of Integrated Traditional Chinese and Western Medicine Nanjing University of Chinese Medicine, Nanjing, Jiangsu 210028, China

² Jiangsu Province Academy of Traditional Chinese Medicine, Nanjing, Jiangsu 210028, China

³ Department of Integrated Chinese and Western Medicine, School of Integrated Chinese and Western Medicine, Nanjing University of Chinese Medicine, Nanjing, Jiangsu 210023, China

⁴ Wang Jing Hospital of CACMS, Beijing 100102, China

⁵ Department of Interventional Radiology, Liyang Hospital of Traditional Chinese Medicine, Liyang, Jiangsu 213399, China

Article Info

Abstract



Article history:

Received: December 10, 2023

Accepted: February 13, 2024

Published: March 31, 2024

Use your device to scan and read the article online



Myocardial fibrosis is a common pathological manifestation that occurs in various cardiac diseases. The present investigation aims to reveal how DNMT1/LncRNA-ANRIL/NLRP3 influences fibrosis and cardiac fibroblast pyroptosis. Here, we used ISO to induce myocardial fibrosis in mice, and LPS and ATP to induce myocardial fibroblast pyroptosis. The results showed that DNMT1, Caspase-1, and NLRP3 expression were significantly increased in fibrotic murine myocardium and pyroptotic cardiac fibroblasts, whereas LncRNA-ANRIL expression was decreased. DNMT1 overexpression decreased the level of LncRNA-ANRIL while increasing the levels of NLRP3 and Caspase-1. Contrarily, silencing DNMT1 increased the LncRNA-ANRIL and decreased the levels of NLRP3 and Caspase-1. Silencing LncRNA-ANRIL increased the levels of NLRP3 and Caspase-1. The present findings suggest that DNMT1 can methylate LncRNA-ANRIL during the development of myocardial fibrosis and CFs cell scorching, resulting in low LncRNA-ANRIL expression, thereby influencing myocardial fibrosis and cardiac fibroblast pyroptosis.

Keywords: DNMT1, Methylation, LncRNA, ANRIL, Myocardial fibrosis, Pyroptosis, NLRP3/Caspase-1 pathway.

1. Introduction

Myocardial fibrosis disrupts normal myocardial architecture, interferes with normal electrophysiological activity, and can also interfere with the rhythmic activity of the myocardium at the corresponding level; this aggravates the pathologic state of heart diseases and causes new pathological changes [1]. Myocardial fibrosis has been shown to significantly increase the mortality of fatal diseases, including atrial fibrillation, sudden death, and heart failure [2]. Cardiac fibroblasts are important factors in the progression of myocardial fibrosis [3].

Pyroptosis is primarily dependent on caspase-1 activation by inflammasomes and specific pattern recognition receptors on the surface or inside of cells that bind to specific ligands, and successively bind to other proteins to form multimeric protein complexes inflammasomes (pyroptosomes), including NOD-like receptor family protein 3 (NLRP3) inflammatory vesicles, and so on [4]. Evidence shows that NLRP3-mediated pyroptosis contributes to myocardial fibrosis [5]. However,

the role of pyroptosis signalling in cardiac fibrosis regulation remains unknown, and more research is required to shed light on this.

LncRNAs are long noncoding RNAs that are longer than 200nt (nucleotides). LncRNAs exert critical roles in chromatin remodelling, transcriptional activation, transcriptional interference, and intranuclear trafficking [6]. LncRNAs also contribute to the initiation and progression of pyroptosis [7]. The antisense non-coding RNA (ANRIL) in the INK4 gene is a lncRNA with 19 exons [8]. ANRIL spans the genome at 126,300 base pairs and is transcribed as a 3834-nt lncRNA [9]. ANRIL is found at 9p21 in the antisense direction within the p15-p16-p14 gene cluster [10]. Experiments demonstrated that LncRNAs abnormalities can cause various diseases, particularly fibrotic diseases [11]. The present experiment revealed that LncRNA-ANRIL was down-regulated in myocardial fibrotic tissue and pyroptotic cardiac fibroblasts. However, the molecular mechanisms underlying the effect of LncRNA-ANRIL on myocardial fibrosis remain largely unknown.

* Corresponding author.

E-mail address: jsszxyxkh@163.com; Kingwei871@163.com (Kaihu Shi, Wei Wang).

These authors contributed equally

Doi: <http://dx.doi.org/10.14715/cmb/2024.70.3.30>

Expression of LncRNAs is regulated by DNA methylation. The methylation of LncRNA-ANRIL promoter is a biomarker for predicting cardiovascular disease risk [12]. DNA methyltransferases catalyze and maintain CpG island hypermethylation in the gene promoter region. DNA methyltransferases 1 (DNMT1) is a DNA methylation transferase that acts on a double DNA strand with one methylated strand to completely methylate it and can participate in the methylation of new synthetic strands in the double strand of DNA replication [13]. Mounting evidence shows that LncRNA binding to DNMT1 potentially influences the methylation of genes involved in myocardial fibrosis [14, 15]. However, whether LncRNA-ANRIL can mediate DNMT1 and affect myocardial fibrosis and the associated mechanisms are elusive.

Therefore, the present study intends to validate whether DNMT1 can modify LncRNA-ANRIL via methylation during the development of myocardial fibrosis and CFs cell scorching, resulting in LncRNA-ANRIL low expression and successively influencing myocardial fibrosis and cardiac fibroblasts pyroptosis.

2. Materials and Methods

2.1. Animal model

Male C57BL/6J SPF grade mice weighing 20 ± 2 g were obtained from Shanghai Slack Laboratory Animals Co., Ltd. (experimental animal production license number: SCXK Hu 2015-0002) and housed at the Experimental Animal Center of the Jiangsu Provincial Academy of Chinese Medicine. The 40 mice were divided randomly into two groups of 20 each, one for control and one for experimentation [16]. The model group ($N = 20$) received daily subcutaneous injections of isoproterenol (ISO; National Medicine Standard: H50020020, purchased from Nanjing, Jiangsu) (5 mg/kg body weight), whereas the control group ($N = 20$) received an equal volume of saline solution. Mice were sacrificed after 14 days, and their hearts were removed. Every heart was divided into two parts, one of which was stored in liquid nitrogen, and the other was fixed in 10% formalin.

2.2. HE staining

A sufficient amount of the fixed sample was placed in a 4% paraformaldehyde solution in the embedding box and then placed in an automatic dehydrator for dehydration. Following complete dehydration, paraffin embedding was performed, and the paraffinized tissue sections were obtained using a manual rotary pathological microtome. The paraffinized tissue slices were placed on an automatic slicer for baking and, 1 hour later, the slices were considered ready; slices were put into the automatic pathological staining machine, and taken out after the specified cycle was run. Finally, the slices were automatically machine-mounted, placed in a fume hood to air dry, taken out the next day, placed in a slicing box, stored at room temperature, and observed and photographed under an optical microscope. We checked at least five random areas of each section and used an automated photo and image analysis system (Image-Pro Plus 6.0, USA) for semi-quantitative evaluation.

2.3. Masson staining

A sufficient amount of the fixed sample was placed in a 4% paraformaldehyde solution in the embedding box and then placed in an automatic dehydrator for dehydration. Following complete dehydration, paraffin embedding was performed, and the paraffinized tissue sections were obtained using a manual

rotary pathological microtome. The paraffinized tissue slices were placed on an automatic slicer for baking and, 1 hour later, the slices were considered ready; slices were stained using the Masson staining kit (BP-DL021, SenBeiJia Biological Technology Co., Ltd., Nanjing, China). Finally, the slices were automatically machine-mounted, placed in a fume hood to air dry, taken out the next day, placed in a slicing box, stored at room temperature, and observed and photographed under an optical microscope. We checked at least five random areas of each section and used an automated photo and image analysis system (Image-Pro Plus 6.0, USA) for semi-quantitative evaluation.

2.4. Sirius red staining

A sufficient amount of the fixed sample was placed in a 4% paraformaldehyde solution in the embedding box and then placed in an automatic dehydrator for dehydration. Following complete dehydration, paraffin embedding was performed, and the paraffinized tissue sections were obtained using a manual rotary pathological microtome. The paraffinized tissue slices were placed on an automatic slicer for baking and, 1 hour later, the slices were considered ready; slices were stained using the Sirius red staining kit (BP-DL030, SenBeiJia Biological Technology Co., Ltd., Nanjing, China). Finally, the slices were automatically machine-mounted, placed in a fume hood to air dry, taken out the next day, placed in a slicing box, stored at room temperature, and observed and photographed under an optical microscope. We checked at least five random areas of each section and used an automated photo and image analysis system (Image-Pro Plus 6.0, USA) for semi-quantitative evaluation.

2.5. Immunohistochemistry (IHC)

The paraffinized tissue slices were placed on an automatic slicer for baking and, 1 hour later, the slices were considered ready. Dewaxed sections were soaked in citrate buffer for 10 minutes before being heated to 100 °C for 10 minutes and blocked in 5 % Bovine albumin Bovine serum albumin solution (BSA) for 1 hour, followed by overnight incubation with primary antibodies at 4°C. Then, the incubated primary antibody was recovered, and the slides were washed with phosphate-buffered saline (PBS) (5 min/cycle, for 3 cycles). After that, the slides were then incubated for 1 hour with the secondary antibody at room temperature. Then, the incubated secondary antibody was recovered, and the slides were washed with PBS (5 min/cycle, for 3 cycles), and successively stained with DAB for 1 min, and re-dyed with hematoxylin. Finally, the sections were dehydrated in ethanol solutions of different concentrations and sealed with neutral resin. Sections of stained specimens were examined at high magnification using a microscope. Five fields were assigned randomly to each segment. ImagePro Plus 6.0 software (U.S.A) was used to quantify the percentage of positive area. All antibody brands and dilution concentrations were as follows: Caspase-1 (83383, CST, 1: 500), DNMT1 (ab188453, Abcam, 1: 500), NLRP3 (15101, CST, 1: 300), Type I collagen (ab260043, Abcam, 1: 500) and Type III collagen (22734-1-AP, Proteintech, 1: 200)

2.6. Cell culture and treatment

One-three day old neonatal C57BL/6J mice were killed and disinfected with 75% alcohol for 10 minutes. The heart was retrieved by opening the chest and cleaned thrice with PBS. Extraneous tissue and vasculature were removed. Mouse heart tissue was minced with scissors. Next, we added 0.25

percent trypsin and 0.1 percent type II collagenase, and the mixture was shaken for 30 minutes in a 37°C thermostat. The suspension was filtered through a 200-mesh filter after digestion. Next, the filtrate was collected and centrifuged. The cells were centrifuged for 5 min at 1000rpm and supernatant was discarded. The cells were grown in a DMEM medium containing 10% foetal bovine serum at 37 °C and 5% CO₂. After two hours of culture, the cells were removed from the medium and replaced with new ones. Cells were divided into control and model groups. After 5.5 hours, 1 µg/ml LPS was added to the model group cells, followed by 5 ng/ml ATP. Cells in the model group were incubated in the same amount of PBS for the same amount of time.

2.7. Plasmid transfection and siRNA transfection

siRNA targeting ANRIL and DNMT1 mRNA, as well as plasmids overexpressing ANRIL and DNMT1, were designed and constructed by Shanghai Jikai Gene Technology Co., Ltd. The cells were digested before they were transferred to six-well culture dishes for incubation. Cells were transfected with RNAimax Lipofectamine (Invitrogen, Carlsbad, CA, USA) at various dosages of siRNA or promiscuous ribonucleic acids as directed by the manufacturer.

2.8. qRT-PCR analysis

RNAiso Plus (9190, TAKARA, Shiga, Japan) was used to lyse the ground mouse heart tissue, which was mixed with chloroform and centrifuged at 12000 rpm for 15 min. After extraction, the supernatant was mixed with isopropanol and centrifuged at 12,000 rpm for 10 min. The supernatant was discarded, and 75% alcohol was used for washing the precipitate. After washing, the supernatant was discarded again and the extracted RNA was dissolved in diethyl pyrocarbonate water. PrimeScript™ RT reagent Kit with gDNA Eraser (RR047A, TAKARA, Shiga, Japan) was used to reverse-transcribe mRNA into cDNA. Finally, the TB Green Premix Ex TaqII kit (RR420A, TAKARA, Shiga, Japan) was used to detect reverse-transcribed cDNA. When the set threshold was reached, the cycle number (CT value) of the fluorescent signal in each reaction tube was recorded. Differences in gene expression were determined using the 2^{-ΔΔCt} method. The sequence of primers was as follows: β-actin (Forward, 5'-CTACCTCATGAAGATCCTGACC-3'; Reverse, 5'-CACAGCTTCTCTTTGATGTCAC-3'), ANRIL (Forward, 5'-TAGCCTCCAGAGTTATCGTCGTT-3'; Reverse, 5'-GCAGAAGTCACCAAGCCTACC-3'), COL1A1 (Forward, 5'-TGAACGTGGTGTACAAGGTC-3'; Reverse, 5'-CCATCTTTACCAGGAGAACCAT-3'), COL3A1 (Forward, 5'-GAAAGAATGGGGAGACTGGAC-3'; Reverse, 5'-TACCAGGTATGCCTTGTAATCC-3'), DNMT1 (Forward, 5'-GAGACGAAAAACGACACGTA-3'; Reverse: 5'-CACTTTGGTGAGTTGATCTTCG-3'), Caspase-1 (Forward, 5'-AGAGGATTTCTTAACGGATGCA-3'; Reverse, 5'-TCACAAGACCAGGCATATTCTT-3'), and NLRP3 (Forward, 5'-GCCGTCTACGTCTTCTTCC-3'; Reverse, 5'-CATCCGACCCAGTGAACAGAG-3')

2.9. Western blotting (WB) analysis

The ground mouse myocardial tissue was lysed with RIPA lysis solution, and centrifuged at 12,000 rpm for 15 min, the supernatant was collected, and the protein concentration was measured using the BCA protein quantification kit. According to the protein concentration, we added the corresponding volume of protein diluent and 5×SDS-loading buffer to ob-

tain a protein concentration of 2 µg/µL. A metal heater was used to heat the mixture at 100°C for 10 min, and the protein sample after heating was used for detection. The gel kit was used to configure a 10% electrophoresis gel separation gel and compression gel. After the configuration was complete, 10 µL of the protein sample was added to the compression gel. The protein electrophoresis gel was then tested and connected to an electrophoresis device. First, electrophoresis was performed at 80V for 30 min and, then, the sample was separated by electrophoresis at 120V. The electrophoresis gel was placed on the transfer membrane device, and the protein was transferred onto a polyvinylidene difluoride (PVDF) membrane (230mA, 2.5 h) that was incubated with 5% BSA solution for 1 h. The PVDF membrane was then cut out according to the different molecular weights of the protein and placed in the antibody-incubation box. The diluted corresponding primary antibody was added for incubation at 4°C overnight. Then, the incubated primary antibody was recovered, and the PVDF membrane was washed with Tris-Buffered Saline and Tween 20 buffer (5 min/cycle, for 3 cycles). After washing the membrane, the corresponding secondary antibody was added to the box and incubated at room temperature for 2 h. After the incubation was completed, TBST was used to clean the PVDF membrane again (5 min/cycle, for 3 cycles). Finally, ECL luminescent solution was used to detect the expression of the corresponding protein bands in the bioimager. ImageJ software was used to analyze the gray value of the protein band, and GAPDH was used as an internal reference to calculate the value. All antibody brands and dilution concentrations were as follows: Caspase-1 (1: 1000), DNMT1 (1: 1000), NLRP3 (1: 1000), Type I collagen (1: 1000) and Type III collagen (1: 1000)

2.10. Hoechst staining

Apoptotic cells were stained with the Hoechst 33258 staining kit (Beyotime). Cells were plated in six-well cell culture plates. The cells were stained using the detection kit according to the manufacturer's instructions. Stained cells were examined using a fluorescence microscope. Five fields from each section were selected randomly. Image-Pro Plus 6.0 software (USA) was employed to quantify densitometric.

2.11. Immunofluorescence (IF)

Cells were cultivated to create cell climbing pieces. After 4% paraformaldehyde treatment, the cells were permeabilized with 0.5 % Triton X-100 for 15 min, blocked for 1 hour with 5% BSA, and then incubated with primary antibodies overnight at 4°C. Then, the incubated primary antibody was recovered, and the slides were washed with PBS (5 min/cycle, for 3 cycles). After washing, the slides were stained with DAPI for 3 minutes after being incubated with the secondary antibody for 1 hour at 37°C in the dark. Finally, the incubated secondary antibody was recovered, and the slides were washed with PBS (5 min/cycle, for 3 cycles). Sections of stained slides were examined using a fluorescence microscope at high magnification. Five fields from each section were randomly selected. ImagePro Plus 6.0 software (USA) was employed for quantification. All antibody dilution concentrations were as follows: Caspase-1 (1: 500), DNMT1 (1: 500), NLRP3 (1: 300), Type I collagen (1: 500) and Type III collagen (1: 200).

3. Results

3.1. Pathological and fibrotic changes in myocardial tissue of mice in an ISO-induced myocardial fibrosis model

We constructed a mouse myocardial fibrosis model by in-

jecting ISO subcutaneously. After two weeks, the HE staining (Fig. 1A), Masson staining (Fig. 1B), and Sirius red staining (Fig. 1C) revealed that the fibrous connective tissue in the ISO-induced myocardial fibrosis proliferated significantly, myocardial cells were significantly deformed, and collagen deposition increased when compared to the control group. Myocardial fibrosis-associated proteins COL1A1 and COL3A1 were detected by qRT-PCR, WB, and IHC. The results revealed that the mRNA expression of COL1A1 and COL3A1 in the myocardial tissue was significantly increased in the mice in the model group two weeks after modeling (Fig. 1E). Moreover, the protein expression of COL1A1 and COL3A1 in the myocardial tissue was significantly increased in mice from the model group (Fig. 1F-G). These findings support the ability of ISO to induce myocardial fibrosis.

3.2. Expression of DNMT1, LncRNA-ANRIL, Caspase-1, NLRP3 and COL1A1, COL3A1 regulation in ISO-induced myocardial fibrosis model in mice

Following ISO induction, qRT-PCR was used to verify LncRNA-ANRIL expression in cardiac tissues. Moreover, the expression of DNMT1, myocardial pyroptosis-related Caspase-1, and NLRP3 was verified by qRT-PCR, western blotting, and immunohistochemistry. The results of qRT-PCR revealed that LncRNA-ANRIL expression in the model group was significantly lower than that in the control group. However, mRNA expression of DNMT1, Caspase-1 and NLRP3 was significantly increased in the cardiac tissue of mice in the model group (Fig. 2A). WB and IHC analysis demonstrated that the model group significantly increased the protein expression of DNMT1, Caspase-1, and NLRP3 (Fig. 2B-C). These findings demonstrate that DNMT1 in myocardial fibrotic tissue can reduce LncRNA-ANRIL expression via methylation, thereby promoting myocardial tissue pyroptosis.

Primary cardiac fibroblasts were extracted, and LPS and ATP were used to construct a cellular pyroptosis model. The expression of COL1A1 and COL3A1 was validated using the model. qRT-PCR results demonstrated significantly lower

mRNA levels of COL1A1 and COL3A1 in pyroptotic cells (Fig. 2D). WB and IF assays indicated significantly more protein levels of COL1A1 and COL3A1 in pyroptotic cells (Fig. 2E-F). These findings demonstrate that LPS and ATP cause CF cellular scorching and promote myocardial fibrosis.

3.3. Expression of DNMT1, LncRNA-ANRIL, and pyroptosis-related proteins in the LPS and ATP-induced pyroptosis model in cardiac fibroblasts

Hochest 33258 was used to analyze apoptotic cells in mouse cardiac fibroblasts after they were treated with LPS. that the analysis revealed that compared to the control group, cardiac fibroblasts induced with LPS and ATP resulted in significantly more apoptotic cells (Fig. 3A). Subsequently, LncRNA-ANRIL expression in cardiac fibroblasts was verified by qRT-PCR after LPS and ATP induction. The expression of DNMT1, Caspase-1 and NLRP3 was verified using qRT-PCR, western blotting, and immunohistochemistry. qRT-PCR analysis revealed significantly lower expression of LncRNA-ANRIL in the model group than in the control group. However, pyroptotic cells significantly increased the mRNA expression of DNMT1, Caspase-1, and NLRP3 in cardiac fibroblasts (Fig. 3B). WB and IF detection results demonstrated that DNMT1, Caspase-1, and NLRP3 protein expression levels were significantly higher in pyroptotic cells (Fig. 3C-D). These findings demonstrate the methylation-induced role of DNMT1 in regulating LncRNA-ANRIL expression during cardiomyocyte pyroptosis.

3.4. Changes in DNMT1, LncRNA-ANRIL expression, and pyroptosis-related proteins in cardiac fibroblasts after overexpression and silencing of DNMT1

DNMT1 was overexpressed in cardiac fibroblasts using

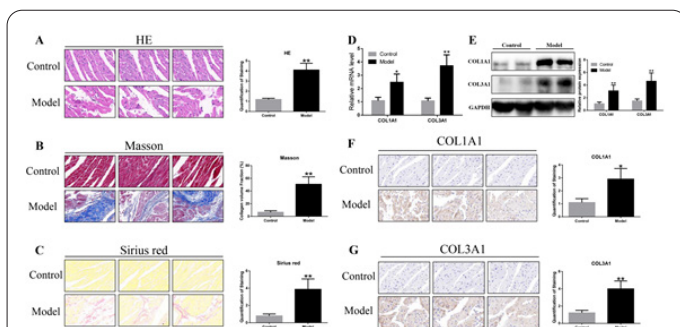


Fig. 1. Pathological and fibrotic changes in myocardial tissue of mice in the ISO-induced myocardial fibrosis model. Myocardial tissues in the HE stained histopathological images (objective: 100×). (B) Myocardial tissues in the Masson-stained histopathological images (objective: 100×). (C) Myocardial tissues in the Sirius red-stained histopathological images (objective: 100×). (D) RT-PCR detection of mRNA levels of COL3A1 and COL1A1 in myocardial tissues. (E) WB assessment of protein levels of COL3A1 and COL1A1 in myocardial tissues. (F) IHC examination of protein levels of COL1A1 in myocardial tissues. (G) IHC examination of protein levels of COL3A1 in myocardial tissues (objective: 100×). Data were shown as mean ± SD ($N = 20$, per group). * $p < 0.05$, ** $p < 0.01$ vs Control.

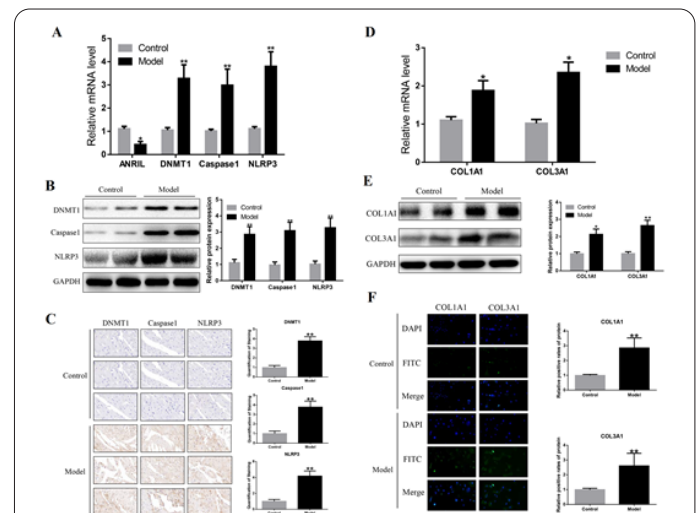
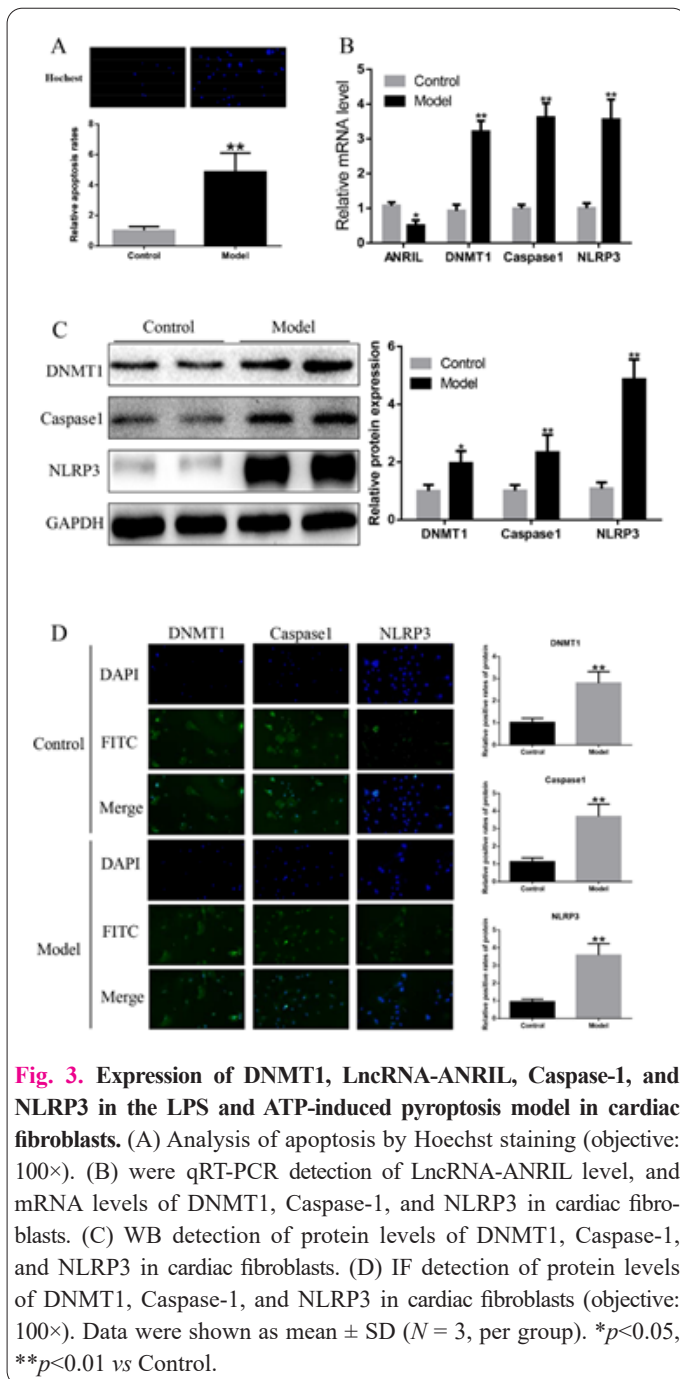


Fig. 2. Expression of DNMT1, LncRNA-ANRIL, Caspase-1, NLRP3 and COL1A1, COL3A1 regulation in ISO-induced myocardial fibrosis model in mice. (A) qRT-PCR detection of the level of LncRNA-ANRIL, and the mRNA levels of DNMT1, Caspase-1, and NLRP3 in cardiac tissues. (B) Western blot analysis of the protein levels of DNMT1, Caspase-1, and NLRP3 in cardiac tissues. (C) IHC analysis of the protein levels of DNMT1, Caspase-1, and NLRP3 in cardiac tissues (objective: 100). (D) RT-PCR detection of mRNA levels of COL3A1 and COL1A1 in cardiac fibroblasts. (E) WB detection of protein levels of COL3A1 and COL1A1 in cardiac fibroblasts. (F) IF analysis of protein levels of COL3A1 and COL1A1 in cardiac fibroblasts (objective: 100×). Data were shown as mean ± SD ($N = 20$, per group). * $p < 0.05$, ** $p < 0.01$ vs Control.



pegFP-C1-DNMT1 and then treated the cells with an empty vector plasmid. qRT-PCR analysis revealed significantly reduced expression of LncRNA-ANRIL in the pEGFP-C1-DNMT1 group following DNMT1 overexpression, whereas the mRNA expression of DNMT1, Caspase-1, and NLRP3 was significantly increased in cardiac fibroblasts (Fig. 5A). WB and IF detection revealed that the protein expression of DNMT1, Caspase-1, and NLRP3 was significantly lower in the pEGFP-C1-DNMT1 group (Fig. 5B-C). Afterward, we used siRNA against DNMT1 to silence DNMT1 expression in pyroptotic cells. qRT-PCR analysis revealed increased expression of LncRNA-ANRIL after silencing DNMT1 in pyroptotic cells, whereas the mRNA expression of DNMT1, Caspase-1, and NLRP3 was significantly decreased in cardiac fibroblasts (Fig. 3D). WB and IF analysis demonstrated the protein expression of DNMT1, Caspase-1, and NLRP3 was significantly lower in cells suppressing DNMT1 than in pyroptotic cells (Fig. 3E-F). These findings show that increased DNMT1 expression plays an important role in decreasing methylation-

regulated LncRNA-ANRIL expression and can cause cardiac fibroblast pyroptosis.

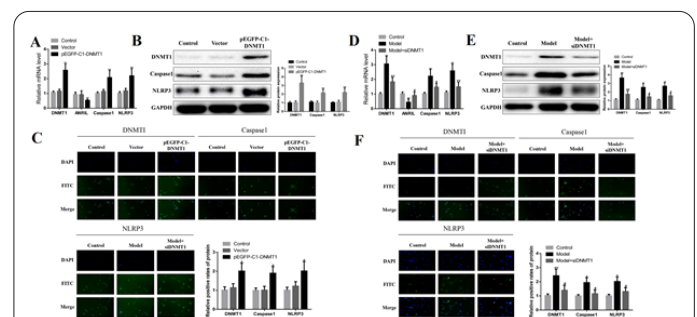
3.5. Changes in LncRNA-ANRIL expression and pyroptosis-related proteins in cardiac fibroblasts after overexpression and silencing of LncRNA-ANRIL.

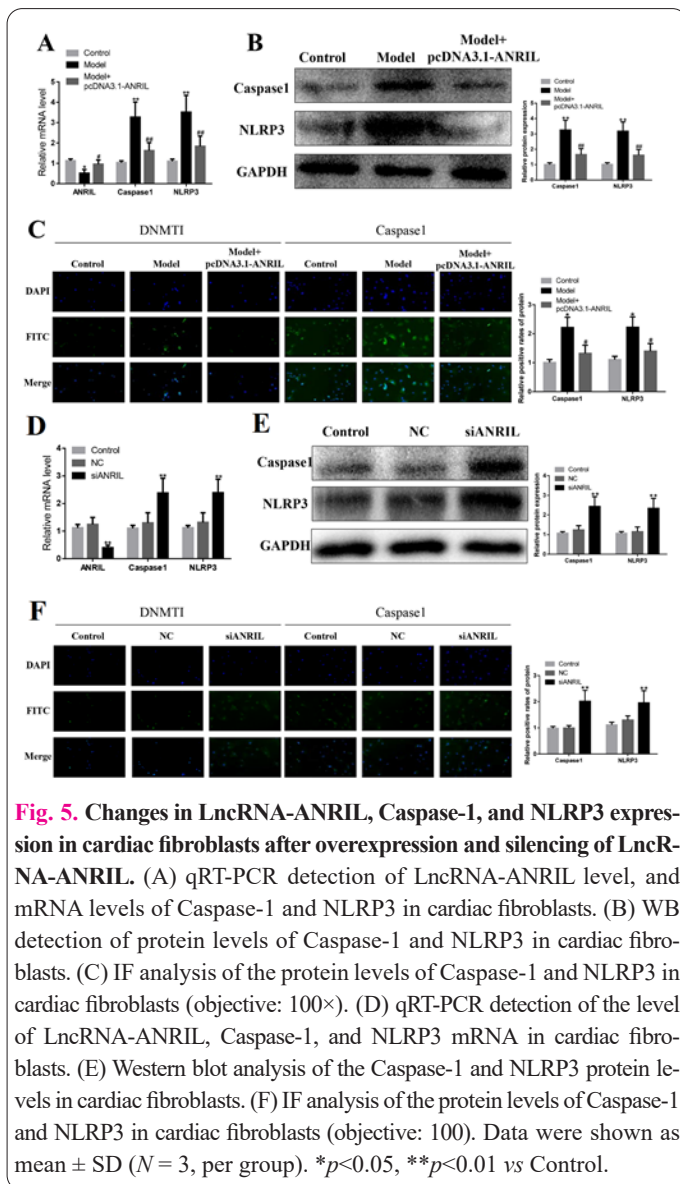
We used pcDNA3.1-ANRIL to overexpress LncRNA-ANRIL in pyroptotic cells. qRT-PCR analysis revealed that LncRNA-ANRIL expression was dramatically increased, whereas Caspase-1 and NLRP3 mRNA expression was significantly decreased in cardiac fibroblasts (Fig. 5A). WB and IF analysis showed that the protein expression of Caspase-1 and NLRP3 was dramatically lower in the pcDNA3.1-ANRIL group compared to pyroptotic cells (Fig. 5B-C). Next, siANRIL was used to silence LncRNA-ANRIL in cardiac fibroblasts. qRT-PCR analysis revealed significantly reduced expression of LncRNA-ANRIL in the siANRIL group after silencing DNMT1, whereas the mRNA expression of Caspase-1 and NLRP3 was significantly increased in cardiac fibroblasts (Fig. 5D). WB and IF analysis demonstrated that the protein expression of Caspase-1 and NLRP3 was significantly reduced in the siANRIL group (Fig. 5E-F). These findings suggest that LncRNA-ANRIL can suppress pyroptosis in cardiac fibroblasts.

4. Discussion

LncRNAs are involved in the development of various disorders and have been linked to cardiovascular disease [17-19]. In epigenetics, DNA methylation affects not only LncRNA expression but also myocardial fibrosis disease, which involves LncRNA [20].

There is no known link between LncRNA and pyroptosis in cardiac fibroblasts during myocardial fibrosis. The goal of this study was to figure out how DNMT1 methylation influences LncRNA-ANRIL regulation, impacting pyroptosis in cardiac fibroblasts. The analysis demonstrated that DNMT1 could inhibit the expression of LncRNA-ANRIL via methylation while also promoting the expression of NLRP3, a pyroptosis-associated inflammasome that contributes to car-





diac fibroblasts pyroptosis and the progression of myocardial fibrosis.

Previous evidence shows that LcnRNA-ANRIL potentially influences not only the process of myocardial fibrosis but also pyroptosis [12, 21, 22]. Low LcnRNA-ANRIL expression promotes autophagy, exacerbates cardiomyocyte blood reperfusion injury, and constitutively aggravates myocardial infarction [23, 24]. Epigenetic silencing of LcnRNA-ANRIL in liver fibrosis increases liver fibrosis and HSC activation via the AMPK pathway [25]. These results support previous findings that DNMT1 methylation inhibited the role of LcnRNA-ANRIL in promoting pyroptosis during myocardial fibrosis.

The expression of LcnRNAs is subjected to a slew of different factors, including DNMT1. Mounting evidence indicates that DNMT1 can inhibit LcnRNA expression by methylating its promoter [26, 27]. DNMT1 also regulates LcnRNA expression in fibrotic diseases [14, 28]. In the present investigation, DNMT1 was found to inhibit LcnRNA-ANRIL expression during myocardial fibrosis and cardiac fibroblast pyroptosis.

NLRP3 is a pyroptotic protein that recognizes pathogen-associated molecular patterns represented by LPS and damage-associated molecular patterns represented by ATP, assembles into inflammasomes, and recruits and activates the pro-inflammatory protease Caspase-1 [29, 30]. Herein, we used LPS and ATP to develop cardiac fibroblast pyroptosis model, confirming that DNMT1 methylation promotes NLRP3-mediated

cardiac fibroblast pyroptosis inhibiting LcnRNA-ANRIL. These findings contribute to the rapidly expanding field of myocardial fibrosis and lay the groundwork for a new theoretical foundation and research path for myocardial fibrosis diagnosis and treatment.

5. Conclusion

The present findings suggest a role for DNMT1 in LcnRNA-ANRIL methylation and increasing the production of NLRP3, a pyroptosis-associated inflammasome, thereby promoting cardiac fibroblast pyroptosis and the progression of myocardial fibrosis.

Informed Consent

The authors report no conflict of interest.

Availability of data and material

We declared that we embedded all data in the manuscript.

Authors' contributions

LZ and GL conducted the experiments and wrote the paper; KC and CX analyzed and organized the data; SK and WW conceived, designed the study and revised the manuscript.

Funding

This work was supported by the Natural Science Foundation of Jiangsu (No. SBK201923150), the Jiangsu Province Academy of Traditional Chinese Medicine Youth Scientific Research Project (No. QNKXYJ202109) the Natural Science Foundation of China Youth Program (No. 82304941).

Acknowledgements

We thanked the Affiliated Hospital of Integrated Traditional Chinese and Western Medicine Nanjing University of Chinese Medicine for approval of our study.

References

- Guo CJ, Ma XK, Xing YH, Zheng CC, Xu YF, Shan L, Zhang J, Wang S, Wang Y, Carmichael GG, Yang L, Chen LL (2020) Distinct Processing of lncRNAs Contributes to Non-conserved Functions in Stem Cells. *Cell* 181 (3): 621-636 e622. doi: 10.1016/j.cell.2020.03.006
- Tian B, Manley JL (2017) Alternative polyadenylation of mRNA precursors. *Nat Rev Mol Cell Biol* 18 (1): 18-30. doi: 10.1038/nrm.2016.116
- Quinn JJ, Zhang QC, Georgiev P, Ilik IA, Akhtar A, Chang HY (2016) Rapid evolutionary turnover underlies conserved lncRNA-genome interactions. *Genes Dev* 30 (2): 191-207. doi: 10.1101/gad.272187.115
- Kesavardhana S, Kanneganti TD (2017) Mechanisms governing inflammasome activation, assembly and pyroptosis induction. *Int Immunol* 29 (5): 201-210. doi: 10.1093/intimm/dxx018
- Tong Y, Wang Z, Cai L, Lin L, Liu J, Cheng J (2020) NLRP3 Inflammasome and Its Central Role in the Cardiovascular Diseases. *Oxid Med Cell Longev* 2020: 4293206. doi: 10.1155/2020/4293206
- Neumann P, Jae N, Knau A, Glaser SF, Fouani Y, Rossbach O, Kruger M, John D, Bindereif A, Grote P, Boon RA, Dimmeler S (2018) The lncRNA GATA6-AS epigenetically regulates endothelial gene expression via interaction with LOXL2. *Nat Commun* 9 (1): 237. doi: 10.1038/s41467-017-02431-1

7. Vento-Tormo R, Alvarez-Errico D, Garcia-Gomez A, Hernandez-Rodriguez J, Bujan S, Basagana M, Mendez M, Yague J, Juan M, Arostegui JJ, Ballestar E (2017) DNA demethylation of inflammasome-associated genes is enhanced in patients with cryopyrin-associated periodic syndromes. *J Allergy Clin Immunol* 139 (1): 202-211 e206. doi: 10.1016/j.jaci.2016.05.016
8. Thomas AA, Feng B, Chakrabarti S (2018) ANRIL regulates production of extracellular matrix proteins and vasoactive factors in diabetic complications. *Am J Physiol Endocrinol Metab* 314 (3): E191-E200. doi: 10.1152/ajpendo.00268.2017
9. Ma J, Li T, Han X, Yuan H (2018) Knockdown of lncRNA ANRIL suppresses cell proliferation, metastasis, and invasion via regulating miR-122-5p expression in hepatocellular carcinoma. *J Cancer Res Clin Oncol* 144 (2): 205-214. doi: 10.1007/s00432-017-2543-y
10. Pahlevan Kakhki M, Nikravesh A, Shirvani Farsani Z, Sahraian MA, Behmanesh M (2018) HOTAIR but not ANRIL long non-coding RNA contributes to the pathogenesis of multiple sclerosis. *Immunology* 153 (4): 479-487. doi: 10.1111/imm.12850
11. Manichaikul A, Wang XQ, Sun L, Dupuis J, Borczuk AC, Nguyen JN, Raghu G, Hoffman EA, Onengut-Gumuscu S, Farber EA, Kaufman JD, Rabinowitz D, Stukovsky KD, Kawut SM, Hunninghake GM, Washko GR, O'Connor GT, Rich SS, Barr RG, Lederer DJ (2017) Genome-wide association study of subclinical interstitial lung disease in MESA. *Respir Res* 18 (1): 97. doi: 10.1186/s12931-017-0581-2
12. Murray R, Bryant J, Titcombe P, Barton SJ, Inskip H, Harvey NC, Cooper C, Lillycrop K, Hanson M, Godfrey KM (2016) DNA methylation at birth within the promoter of ANRIL predicts markers of cardiovascular risk at 9 years. *Clin Epigenetics* 8: 90. doi: 10.1186/s13148-016-0259-5
13. Milillo A, Molinario C, Costanzi S, Vischini G, La Carpia F, La Greca F, Rigante D, Gambaro G, Gurrieri F, Sangiorgi E (2018) Defective activation of the MAPK/ERK pathway, leading to PARP1 and DNMT1 dysregulation, is a common defect in IgA nephropathy and Henoch-Schonlein purpura. *J Nephrol* 31 (5): 731-741. doi: 10.1007/s40620-018-0482-6
14. She Q, Shi P, Xu SS, Xuan HY, Tao H, Shi KH, Yang Y (2020) DNMT1 Methylation of lncRNA GAS5 Leads to Cardiac Fibroblast Pyroptosis via Affecting NLRP3 Axis. *Inflammation* 43 (3): 1065-1076. doi: 10.1007/s10753-020-01191-3
15. Yang JJ, She Q, Yang Y, Tao H, Li J (2018) DNMT1 controls lncRNA H19/ERK signal pathway in hepatic stellate cell activation and fibrosis. *Toxicol Lett* 295: 325-334. doi: 10.1016/j.toxlet.2018.07.013
16. Shi P, Zhao XD, Shi KH, Ding XS, Tao H (2021) MiR-21-3p triggers cardiac fibroblasts pyroptosis in diabetic cardiac fibrosis via inhibiting androgen receptor. *Exp Cell Res* 399 (2): 112464. doi: 10.1016/j.yexcr.2020.112464
17. Thum T (2014) Noncoding RNAs and myocardial fibrosis. *Nat Rev Cardiol* 11 (11): 655-663. doi: 10.1038/nrcardio.2014.125
18. Tao H, Song ZY, Ding XS, Yang JJ, Shi KH, Li J (2018) lncRNAs and miRNAs as epigenetic signatures in diabetic cardiac fibrosis: new advances and perspectives. *Endocrine* 62 (2): 281-291. doi: 10.1007/s12020-018-1688-z
19. Kumar A, Thomas SK, Wong KC, Lo Sardo V, Cheah DS, Hou YH, Placone JK, Tenerelli KP, Ferguson WC, Torkamani A, Topol EJ, Baldwin KK, Engler AJ (2019) Mechanical activation of noncoding-RNA-mediated regulation of disease-associated phenotypes in human cardiomyocytes. *Nat Biomed Eng* 3 (2): 137-146. doi: 10.1038/s41551-018-0344-5
20. Tao H, Song ZY, Ding XS, Yang JJ, Shi KH, Li J (2018) Epigenetic signatures in cardiac fibrosis, special emphasis on DNA methylation and histone modification. *Heart Fail Rev* 23 (5): 789-799. doi: 10.1007/s10741-018-9694-z
21. Zhang L, Wang YM (2019) Expression and function of lncRNA ANRIL in a mouse model of acute myocardial infarction combined with type 2 diabetes mellitus. *J Chin Med Assoc* 82 (9): 685-692. doi: 10.1097/JCMA.000000000000182
22. Wang J, Zhao SM (2021) lncRNA-antisense non-coding RNA in the INK4 locus promotes pyroptosis via miR-497/thioredoxin-interacting protein axis in diabetic nephropathy. *Life Sci* 264: 118728. doi: 10.1016/j.lfs.2020.118728
23. Han Y, Wang H, Wang Y, Dong P, Jia J, Yang S (2021) Puerarin protects cardiomyocytes from ischemia-reperfusion injury by upregulating lncRNA ANRIL and inhibiting autophagy. *Cell Tissue Res* 385 (3): 739-751. doi: 10.1007/s00441-021-03463-2
24. Song B, Wei D, Yin G, Song X, Wang S, Jia S, Zhang J, Li L, Wu X (2021) Critical role of SIRT1 upregulation on the protective effect of lncRNA ANRIL against hypoxia/reoxygenation injury in H9c2 cardiomyocytes. *Mol Med Rep* 24 (2). doi: 10.3892/mmr.2021.12186
25. Yang JJ, Yang Y, Zhang C, Li J, Yang Y (2020) Epigenetic silencing of lncRNA ANRIL enhances liver fibrosis and HSC activation through activating AMPK pathway. *J Cell Mol Med* 24 (4): 2677-2687. doi: 10.1111/jcmm.14987
26. Pan Z, Zhong B, Ling X, Zhang H, Tan Q, Huang D, Chen J, Zhang H, Zheng D, Li H, Chen X, Liu L (2021) The DNMT1-associated lncRNA UCA1 was upregulated in TK6 cells transformed by long-term exposure to hydroquinone and benzene-exposed workers via DNA hypomethylation. *J Biochem Mol Toxicol*: e22920. doi: 10.1002/jbt.22920
27. Lei Y, Xu Y, Li XF, Chen Y (2021) Coexpression Network Analysis of lncRNA Associated with Overexpression of DNMT1 in Esophageal Epithelial Cells. *Biomed Res Int* 2021: 7162270. doi: 10.1155/2021/7162270
28. Xue R, Li Y, Li X, Ma J, An C, Ma Z (2019) miR-185 affected the EMT, cell viability, and proliferation via DNMT1/MEG3 pathway in TGF-beta1-induced renal fibrosis. *Cell Biol Int* 43 (10): 1152-1162. doi: 10.1002/cbin.11046
29. Gaul S, Leszczynska A, Alegre F, Kaufmann B, Johnson CD, Adams LA, Wree A, Damm G, Seehofer D, Calvente CJ, Povero D, Kisseleva T, Eguchi A, McGeough MD, Hoffman HM, Pellegrin P, Laufs U, Feldstein AE (2021) Hepatocyte pyroptosis and release of inflammasome particles induce stellate cell activation and liver fibrosis. *J Hepatol* 74 (1): 156-167. doi: 10.1016/j.jhep.2020.07.041
30. Lv X, Fan C, Jiang Z, Wang W, Qiu X, Ji Q (2021) Isoliquiritigenin alleviates P. gingivalis-LPS/ATP-induced pyroptosis by inhibiting NF-kappaB/ NLRP3/GSDMD signals in human gingival fibroblasts. *Int Immunopharmacol*: 108338. doi: 10.1016/j.intimp.2021.108338